

Probing compressed triplet scalars with ISR jets and soft leptons at the LHC

Atri Dey^{a*} , Tathagata Ghosh^{b†} , Biswarup Mukhopadhyaya^{c‡}, Agnivo Sarkar^{b,§} 

^a*Department of Physics and Astronomy, Uppsala University, Box 516, SE-751 20 Uppsala, Sweden*

^b*Regional Centre for Accelerator-based Particle Physics, Harish-Chandra Research Institute,
A CI of Homi Bhabha National Institute, Chhatnag Road, Jhansi, Prayagraj 211019, India*

^c*Department of Physical Sciences, Indian Institute of Science Education and Research Kolkata,
Mohanpur, 741246, India.*

Abstract

The Type-II seesaw model predicts doubly and singly charged scalars along with neutral Higgs states originating from an $SU(2)$ triplet. Current LHC searches by the ATLAS and CMS collaborations constrain these particles mainly under the assumption that the doubly charged scalar decays dominantly into same-sign dileptons or dibosons. However, when moderate mass splittings exist among the triplet scalars, cascade decays can dominate, suppressing these conventional search channels and leaving sizeable regions of parameter space weakly constrained. We study this compressed region characterized by $1 \text{ GeV} \lesssim \Delta M \lesssim 30 \text{ GeV}$ and triplet vev $v_t \sim 10^{-7} - 10^{-3} \text{ GeV}$. In this scenario, charged scalars predominantly undergo cascade decays, while neutral scalars decay invisibly into neutrinos, leading to final states with soft leptons and missing transverse energy. We propose a dedicated search strategy at the 14 TeV LHC exploiting a hard initial-state radiation jet to boost the scalar system. Using a cut-and-count analysis, we show that discovery-level sensitivity can be achieved in this previously unexplored region with an integrated luminosity of 3000 fb^{-1} . Our results signify the importance of dedicated searches targeting cascade-dominated and compressed mass spectrum for beyond the standard model scenarios with an $SU(2)$ multiplet.

*atridehy1993@gmail.com, atri.dey@physics.uu.se

†tathagataghosh@hri.res.in

‡biswarup@iiserkol.ac.in

§agnivosarkar@hri.res.in

1 Introduction

The standard model (SM) of particle physics fails to provide a satisfactory explanation for the observed neutrino masses and mixing. To resolve this shortcoming, the Type-II seesaw mechanism [1–6] offers a well-motivated theoretical framework which is a minimal extension of the SM. In this beyond the standard model (BSM) scenario, the scalar sector is extended with a $SU(2)_L$ triplet field (Δ) with hypercharge $Y = 2$ in addition to the usual SM-like scalar doublet (Φ). The doublet field acquires a vacuum expectation value (vev) v_d at the electroweak scale and breaks the electroweak symmetry spontaneously. As a consequence, the triplet vev v_t is induced through a trilinear scalar interaction of the form $\Lambda(\Phi^T i\sigma_2 \Delta^\dagger \Phi + h.c.)$, where Λ is a potential parameter with mass dimension one. After spontaneous symmetry breaking, the scalar spectrum of the model consists of a pair of doubly charged ($H^{\pm\pm}$) and singly charged (H^\pm) Higgs bosons, along with three neutral Higgs states. Of the neutral scalars, two are CP-even (H^0, h^0), while one is CP-odd (A^0). In general, the lightest CP-even scalar state h^0 is identified with the observed SM-like Higgs boson with mass 125 GeV, which was discovered by the ATLAS and CMS collaborations at the LHC [7–10]. The gauge symmetry of the model allows the scalar triplet to couple directly with the left-handed lepton doublets. After symmetry breaking, the neutral CP-even component of the Δ field acquires a small but non-zero vev , which in turn generates Majorana neutrino masses via the seesaw mechanism. An important phenomenological implication of this BSM scenario is the presence of various exotic scalars, particularly the doubly charged Higgs bosons, which give rise to tantalizing signatures at collider experiments.

Both ATLAS and CMS collaborations [11–21] have performed extensive searches for doubly charged scalars ($H^{\pm\pm}$) which dominantly produced via different electroweak processes in a model-agnostic manner. Typically these production mechanisms at the LHC include Drell-Yan pair production as well as single production via Vector Boson fusion (VBF) channels¹. Due to their distinctive electric charges, the $H^{\pm\pm}$ can generate interesting final states with relatively low SM backgrounds. Following production, the doubly charged scalars can decay either into same-sign dilepton pairs or into a pair of same-sign W bosons, depending on the underlying model parameters. To be specific, for the Type-II seesaw model, the dominant production mode is determined by the triplet vev v_t . In the leptonic decay scenario ($v_t \leq 10^{-5}$ GeV), assuming an equal branching ratio into all possible same-flavor and mixed-flavor final states, $BR(H^{\pm\pm} \rightarrow e^\pm e^\pm) = BR(H^{\pm\pm} \rightarrow \mu^\pm e^\pm) = BR(H^{\pm\pm} \rightarrow e^\pm \tau^\pm) = BR(H^{\pm\pm} \rightarrow \mu^\pm \mu^\pm) = BR(H^{\pm\pm} \rightarrow \mu^\pm \tau^\pm) = BR(H^{\pm\pm} \rightarrow \tau^\pm \tau^\pm)$ the ATLAS collaboration [21] has placed a lower bound on the $H^{\pm\pm}$ mass of approximately $m_{H^{\pm\pm}} \lesssim 1080$ GeV. Apart from the leptonic modes, the $H^{\pm\pm}$ can also decay into pair of same sign W boson, $H^{\pm\pm} \rightarrow W^\pm W^\pm$, which becomes particularly dominant for larger value of v_t ($v_t \geq 10^{-3}$ GeV). For this scenario, dedicated searches exclude $m_{H^{\pm\pm}}$ masses in the range of 200 GeV - 350 GeV [20] depending upon different modes of W -boson decay.

Several recent studies [22–27] have reinterpreted existing experimental limits to derive the bounds on the parameter space relevant for the scalar sector of the Type-II seesaw model. From their analysis, one can determine the current lower limit on the mass of the doubly charged scalar. As discussed before, these limits primarily depend on the assumption that $H^{\pm\pm}$ decays via a pair of same-sign dilepton or a pair of same-sign W boson modes. Interestingly, lower limits on the $H^{\pm\pm}$ mass can be significantly relaxed if one considers relative mass gap between the triplet scalars. In this choice the

¹The CMS collaboration has searched for the single production of $H^{\pm\pm}$ states that are produced via VBF mode and subsequently decay into same-sign WW final state [14]. In this process, both the production and decay vertices are controlled by $H^{\pm\pm} W^\mp W^\mp$ coupling. In the case of the Type-II seesaw model, this coupling is proportional to the ratio between the doublet and triplet vev $\frac{v_t}{v_d}$. In the following, we will describe the present BSM scenario $v_t \ll v_d$. As a result, this will impose relatively weaker constraints in the model parameter space.

cascade decay modes among the triplet scalars open up and can appear as dominant channels for a range of v_t values.

To explain the cascade decay mode for the $H^{\pm\pm}$ we like to point out that the scalar sector of this BSM framework is largely governed by three parameters - the mass of the doubly charged scalar $m_{H^{\pm\pm}}$, the mass gap $\Delta M = m_{H^{\pm\pm}} - m_{H^\pm} = m_{H^\pm} - m_{H/A}$ and the triplet vev v_t . Now for a moderate value of ΔM (and $v_t \sim 10^{-7} - 10^{-3}$ GeV), the $H^{\pm\pm}$ can decay via $H^{\pm\pm} \rightarrow H^\pm W^*$. In Ref. [28], the authors have shown that for a moderate mass gap, which is delineated as $1 \text{ GeV} \lesssim \Delta M \lesssim 30 \text{ GeV}$, the charged triplet scalars can predominantly decay via cascade modes. As a consequence, the aforementioned conventional channels that are analysed in different direct search experiments have suppressed branching ratios. In addition, for $v_t \leq 10^{-4}$ GeV, both the neutral BSM scalars can decay via the $\bar{\nu}^c \nu$ mode. As a result, a non-trivial region of parameter space, which is described as $\Delta M \gtrsim 10$ GeV and $v_t \sim 10^{-7} - 10^{-3}$ GeV remains effectively unconstrained by the existing limits.

Here, we would like to emphasise why this aforementioned region is challenging to probe.

- The widths for both $H^{\pm\pm} \rightarrow \ell^\pm \ell^\pm$ and $H^{\pm\pm} \rightarrow W^\pm W^\pm$ decays are relatively small. Hence, $H^{\pm\pm}$ mainly decay in the channel $H^{\pm\pm} \rightarrow W^* H^\pm$. Similarly, the singly charged scalar dominantly decays in the $H^\pm \rightarrow W^* H^0/A^0$ channel. Finally, in the aforementioned unconstrained region, all the neutral triplet scalars exclusively decays into $H^0/A^0 \rightarrow \bar{\nu}^c \nu$ mode.
- The triplet scalar mass spectrum is compressed. Hence, the W^\pm bosons which are resulting from cascade decays of charged scalars are kinematically off-shell. As a result, visible daughter jets and leptons which are generated in the subsequent decays are also very soft. Recently, Ref. [29] has presented an analysis that targets this parameter space. In this work, the authors have focused on a pair of same-sign lepton final states. However, we find the combined trigger, which corresponds to the pair of lepton, which is used in their study, to be unrealistic.
- In our work, we use the missing energy E_T^{miss} trigger, which is proven to be effective in probing the compressed mass spectra scenario. We demand at least one jet with sufficiently large p_T from initial state radiation. This provide large boosts to decaying particle pairs and also a large E_T^{miss} . For our analysis, we consider one jet and two soft leptons along with missing energy as our final state signature.

All these reasons motivate us to formulate a dedicated collider search strategy aimed at probing this exclusive parameter region. Our study can extend the existing experimental sensitivity of Type-II scenarios beyond existing limits.

This paper is organized as follows. In Sec. (2), we briefly describe the scalar sector of the Type-II seesaw model. After that, we determine the benchmark scenarios are safe from existing experiments and present them in Sec. (3). Furthermore, in Sec. (4), we present our analysis strategy, including the definition of selection cuts and a cut-and-counts analysis, and discuss the resulting signal significance. Finally, we summarize our findings in Sec. (5).

2 A Brief Description of the Seesaw Scalar Sector

In this section, we present the essential aspects of the Type-II seesaw model with particular attention to its scalar sector. In addition to the SM-like scalar doublet Φ , this model contains an additional $SU(2)_L$ scalar triplet field Δ with hypercharge $Y = 2$. In gauge basis, the triplet and doublet fields can be written in the following manner:

$$\Delta = \begin{bmatrix} \delta^+/\sqrt{2} & \delta^{++} \\ \delta^0 & -\delta^+/\sqrt{2} \end{bmatrix} \quad \text{and} \quad \Phi = \begin{bmatrix} \phi^+ \\ \phi^0 \end{bmatrix}. \quad (1)$$

In Eq. (2) we write down the gauge invariant scalar potential following the notation described in Ref. [30,31].

$$\begin{aligned}
V(\Phi, \Delta) = & -\mu^2 \Phi^\dagger \Phi + \frac{\lambda}{2} (\Phi^\dagger \Phi)^2 + \widetilde{M}_\Delta^2 \text{Tr} (\Delta^\dagger \Delta) + \frac{\lambda_1}{2} \text{Tr} [(\Delta^\dagger \Delta)]^2 \\
& + \frac{\lambda_2}{2} \left(\text{Tr} [(\Delta^\dagger \Delta)]^2 - \text{Tr} [(\Delta^\dagger \Delta)^2] \right) + \lambda_4 (\Phi^\dagger \Phi) \text{Tr} (\Delta^\dagger \Delta) + \lambda_5 \Phi^\dagger [\Delta^\dagger, \Delta] \Phi \\
& + \left(\frac{\Lambda_6^i}{\sqrt{2}} \Phi^T \sigma_2 \Delta^\dagger \Phi + \text{h.c.} \right).
\end{aligned} \tag{2}$$

Here μ^2 , \widetilde{M}_Δ^2 , and Λ_6 denote the dimension-full mass parameters appearing in the scalar potential. The quartic couplings λ and λ_i are independent dimensionless parameters and, without loss of generality, can be considered to be real by assuming an appropriate phase redefinition of the triplet field Δ . The neutral component of the Φ field acquires a non-zero vev v_d , thereby triggering electroweak symmetry breaking. The trilinear interaction term involving Λ_6 in Eq. (2) induces a tadpole term for the triplet field, which subsequently generates a non-zero vev v_t for the neutral component of Δ . Minimising the scalar potential w.r.t. the neutral scalar fields, leads to two independent tadpole conditions, as given below. These identities relate the dimension-full scalar parameters to the doublet vev v_d and triplet vev v_t respectively.

$$\begin{aligned}
\mu^2 &= \frac{\lambda}{2} v_d^2 - \Lambda_6 v_t + \frac{1}{2} (\lambda_4 - \lambda_5) v_t^2 \\
\widetilde{M}_\Delta^2 &= \frac{\Lambda_6 v_d^2}{2v_t} - \frac{\lambda_1}{2} v_t^2 - \frac{1}{2} (\lambda_4 - \lambda_5) v_d^2
\end{aligned} \tag{3}$$

These conditions will be useful to determine the mass eigenvalue of different scalar fields. The gauge interaction of these scalar fields is governed by their corresponding covariant derivatives -

$$\begin{aligned}
D_\mu \Phi &= \left(\partial_\mu - i \frac{g}{2} \sigma^a W_\mu^a - i \frac{g'}{2} B_\mu \right) \Phi, \\
D_\mu \Delta &= \partial_\mu \Delta - i \frac{g}{2} [\sigma^a W_\mu^a, \Delta] - i \frac{g'}{2} B_\mu \Delta,
\end{aligned} \tag{4}$$

where g , g' are the $SU(2)_L$ and $U(1)_Y$ gauge couplings respectively. After electroweak symmetry breaking, the kinetic terms $(D_\mu \Phi)^\dagger (D^\mu \Phi)$ and $\text{Tr}[(D_\mu \Delta)^\dagger (D^\mu \Delta)]$ generate the mass terms for the electroweak gauge bosons with both v_d and v_t are contributing to the W and Z boson masses. At the tree level, these masses can be expressed as

$$M_W^2 = \frac{g^2}{4} (v_d^2 + 2v_t^2), \quad M_Z^2 = \frac{g^2 + g'^2}{2} (v_d^2 + 4v_t^2) \tag{5}$$

The corresponding tree level ρ parameter in this model takes the following form

$$\rho \equiv \frac{M_W^2}{M_Z^2 \cos^2 \theta_W} = \frac{v_d^2 + 2v_t^2}{v_d^2 + 4v_t^2}. \tag{6}$$

From precision electroweak data, the measured value of the ρ parameter is $\rho = 1.00038(20)$ [32]. To satisfy this, the tree-level value of the ρ parameter has to be very close to unity. Using this fact,

one can obtain the upper limit on the triplet vev $v_t \lesssim 0.78$ GeV at 2σ . Consequently, we work in the phenomenologically viable limit $v_t \ll v_d$ and identify $v_d \rightarrow v$, where $v \simeq 246$ GeV denotes the electroweak vev . In this limit, the tadpole Eq. (3) can further be simplified and re-expressed in the following manner -

$$v_t = \frac{\Lambda_6 v^2}{2\widetilde{M}_\Delta^2 + v^2(\lambda_4 - \lambda_5)}. \quad (7)$$

The gauge symmetry of the model allows us to write down the Yukawa interaction term between the scalar triplet Δ and the SM lepton doublets $L = (\nu_L, \ell_L)^T$ in the following manner:

$$\mathcal{L}_\nu = Y_\nu^\nu L_i^T C i \sigma_2 \Delta L_j + h.c. \quad (8)$$

Here Y^ν is the complex symmetric matrix, i and j are the flavor indices, and C denotes the charge conjugation operator. One can realise that the triplet vev v_t can generate Majorana mass terms for the neutrinos. The resulting neutrino mass matrix can be expressed as $m_{ij}^\nu = \sqrt{2} Y_{ij}^\nu v_t$. This mass matrix can be diagonalized using the Pontecorvo–Maki–Nakagawa–Sakata (PMNS) matrix (U_{PMNS}), which encodes the observed neutrino mixing angles and CP-violating phases. Explicitly, U_{PMNS} contains three mixing angles ($\theta_{12}, \theta_{13}, \theta_{23}$), on Dirac CP phase δ_{CP} and two Majorana phase (α_1, α_2) such that $m_{ij}^\nu = U_{PMNS} m_\nu^{diag} U_{PMNS}^T$. Given a specific triplet vev v_t and the low-energy neutrino data, this relation allows one to reconstruct the structure of the Yukawa coupling matrix Y_ν . For the present study, we adopt the best-fit values of the neutrino oscillation parameters from Ref. [33].

After electroweak symmetry breaking, the neutral scalar states ϕ^0 and δ^0 mix to form two CP-even states, h^0 and H^0 and two CP-odd state G^0 and A^0 with the mixing angle α and β_0 respectively. In the following, we identify the lighter CP-even state h^0 as the observed SM-like Higgs boson. Similarly, the singly charged states ϕ^\pm and δ^\pm mix into the mass eigenstates G^\pm and H^\pm with a mixing angle β_\pm . In contrast to that, the doubly charged scalar gauge states $\delta^{\pm\pm}$ are already aligned with the mass eigenstates $H^{\pm\pm}$. Hereafter, we use $H^{\pm\pm}$ to denote the doubly charged Higgs boson. The Goldstone modes G^0 and G^\pm are absorbed by the Z and W bosons, respectively, providing their longitudinal components and thereby giving them mass. The relationship between the gauge eigenstates and the corresponding mass eigenstates can be expressed as:

$$\begin{aligned} H^{\pm\pm} &= \delta^{\pm\pm} \\ \begin{bmatrix} G^\pm \\ H^\pm \end{bmatrix} &= \begin{bmatrix} \cos \beta_\pm & \sin \beta_\pm \\ -\sin \beta_\pm & \cos \beta_\pm \end{bmatrix} \begin{bmatrix} \phi^\pm \\ \delta^\pm \end{bmatrix} \\ \begin{bmatrix} G^0 \\ A^0 \end{bmatrix} &= \begin{bmatrix} \cos \beta_0 & \sin \beta_0 \\ -\sin \beta_0 & \cos \beta_0 \end{bmatrix} \begin{bmatrix} \text{Im}[\phi^0] \\ \text{Im}[\delta^0] \end{bmatrix} \\ \begin{bmatrix} h^0 \\ H^0 \end{bmatrix} &= \begin{bmatrix} \cos \alpha & \sin \alpha \\ -\sin \alpha & \cos \alpha \end{bmatrix} \begin{bmatrix} \text{Re}[\phi^0] \\ \text{Re}[\delta^0] \end{bmatrix} \end{aligned} \quad (9)$$

where the mixing angles are defined as

$$\tan \beta_0 = \sqrt{2} \tan \beta_\pm = \frac{2v_t}{v_d} \quad \text{and} \quad \tan 2\alpha = \frac{4v_t}{v_d} \frac{(\widetilde{M}_\Delta^2 + \frac{1}{2}\lambda_1 v_t^2)}{\widetilde{M}_\Delta^2 + \frac{3}{2}\lambda_1 v_t^2 + \frac{1}{2}(\lambda_4 - \lambda_5 - 2\lambda)v_t^2} \quad (10)$$

In the limit $v_t \ll v_d$, one of the mixing angles and the masses of the BSM scalars² would take the following simplified form -

$$\begin{aligned}
m_{H^{\pm\pm}}^2 &\simeq \widetilde{M}_\Delta^2 + \frac{1}{2}(\lambda_4 + \lambda_5)v_d^2 \\
m_{H^\pm}^2 &\simeq \widetilde{M}_\Delta^2 + \frac{1}{2}\lambda_4 v_d^2 \\
m_{A^0/H^0}^2 &\simeq \widetilde{M}_\Delta^2 + \frac{1}{2}(\lambda_4 - \lambda_5)v_d^2 \\
\tan 2\alpha &\simeq \frac{4v_t}{v_d} \left(1 - \frac{m_{h^0}^2}{m_{H^0}^2}\right)^{-1} \\
M_\Delta^2 &= \widetilde{M}_\Delta^2 + \frac{\lambda_4}{2}v_d^2
\end{aligned} \tag{11}$$

From Eq(11), one can realise that the mass-squared difference between these BSM scalars can be expressed as -

$$m_{H^{\pm\pm}}^2 - m_{H^\pm}^2 = m_{H^\pm}^2 - m_{H^0/A^0}^2 = \frac{\lambda_5}{2}v_d^2. \tag{12}$$

For our later discussion, we would introduce a new parameter which encodes the mass splitting between these BSM scalars - $\Delta M = m_{H^{\pm\pm}} - m_{H^\pm} = m_{H^\pm} - m_{H^0/A^0}$. Before concluding this section, we would like to mention the theoretical constraints on these scalar parameters. Demanding perturbative unitarity and stability, one can determine these theoretical constraints on the quartic couplings of the scalar potential. The necessary and sufficient conditions for the potential to be bounded-from-below (BFB) Ref. [31] are given as

$$\begin{aligned}
\lambda \geq 0, \quad \lambda_1 \geq 0, \quad 2\lambda_1 + \lambda_2 \geq 0, \quad \lambda_4 \pm \lambda_5 + \sqrt{\lambda\lambda_1} \geq 0, \quad 2|\lambda_5|\sqrt{\lambda_1 + \lambda_2}\sqrt{\lambda} \geq 0, \\
\lambda_4 + \sqrt{(\lambda\lambda_2 + 2\lambda_5^2)(\lambda_1/\lambda_2 + 1/2)} \geq 0, \quad \lambda_4 \pm \lambda_5 + \sqrt{\lambda(\lambda_1 + \frac{\lambda_2}{2})} \geq 0
\end{aligned} \tag{13}$$

Along with that, another set of constraints on scalar potential parameters can be determined by demanding tree-level unitarity to be preserved, while considering different tree level $2 \rightarrow 2$ scattering processes: scalar-scalar scatterings, gauge boson scatterings, and scalar-gauge boson scatterings. For the Type-II seesaw model, to ensure perturbative unitarity. scalar parameters must obey the following conditions [31]

$$\begin{aligned}
\lambda \leq \frac{8}{3}\pi, \quad \lambda_1 - \lambda_2 \leq 8\pi, \quad 4\lambda_1 + \lambda_2 \leq 8\pi, \quad 2\lambda_1 + 3\lambda_2 \leq 16\pi \\
|\lambda_5| \leq \frac{1}{2} \min \left[\sqrt{(\lambda \pm 8\pi)(\lambda_1 - \lambda_2 \pm 8\pi)} \right] \\
|\lambda_4| \leq \frac{1}{\sqrt{2}} \sqrt{(\lambda - \frac{8}{3}\pi)(4\lambda_1 + \lambda_2 - 8\pi)}
\end{aligned} \tag{14}$$

3 Constraints and Benchmarks

From the discussion in the previous section and Eq. (12), it follows that the mass-splitting parameter can take either positive or negative values depending on the value of λ_5 . Both these choice of λ_5 values

²One can realise that in this limit, both $\tan \beta_0$ and $\tan \beta_\pm$ are very small. Here we fix the corresponding values at $\mathcal{O}(10^{-8})$ and light CP -even scalar mass becomes $m_{h^0}^2 \simeq 2\lambda v_d^2$.

which are compatible with the theoretical constraints that are illustrated in Eq. (13) and Eq. (14) respectively. Based upon the ΔM parameter one can expect three possible scenarios: (i) **Degenerate Scenario** ($\Delta M \simeq 0$): $m_{H^{\pm\pm}} \simeq m_{H^\pm} \simeq m_{H^0/A^0}$ (ii) **Positive Hierarchy Scenario** ($\Delta M > 0$): $m_{H^{\pm\pm}} > m_{H^\pm} > m_{H^0/A^0}$ and (iii) **Negative Hierarchy Scenario** ($\Delta M < 0$): $m_{H^{\pm\pm}} < m_{H^\pm} < m_{H^0/A^0}$. With these definitions in hand, we now elaborate on the phenomenological aspects of these BSM scalars. One can notice that all the potential parameters can be expressed in terms of the bare mass term³ (M_Δ), ΔM , v_t , and the mixing angle α . For all practical purposes, we can consider these as the fundamental parameters to analyze the phenomenological features of the scalar sector for this BSM scenario. Here, we present the existing constraints on these parameters which are coming from different experiments.

To impose the bound on mixing angle α , one can demand that the coupling between h^0 and other SM particles must remain within the SM expectation value. In addition, the presence of the additional charged scalars in this model can enhance the branching ratio of $h^0 \rightarrow \gamma\gamma$ through loop-mediated contributions. However, to ensure that the properties of h^0 is compatible with the recent LHC measurements, the corresponding values of the mixing angle must satisfy the limit $|\sin \alpha| \lesssim 0.3$ [24, 34].

The electroweak precision observables, which are parametrised by the oblique coefficients (S , T , and U), receive additional contributions due to the presence of exotic scalar bosons. For this model, the current measurement on the T parameter strictly disfavours the large mass difference between the triplet scalars. To satisfy this limit, one can impose the bound $|\Delta M| \lesssim 40$ GeV [24, 35, 36]. For our numerical analysis, we take the best-fitted value for the S and T parameters provided by the Gfitter Group: $S = 0.06 \pm 0.09$ and $T = 0.10 \pm 0.07$ with a correlation coefficient of +0.91 [37].

The interaction Lagrangian as described in Eq. (8) can give rise to different lepton flavor violating (LFV) processes, $\ell_\alpha \rightarrow \ell_\beta \gamma$ which are generated via both H^\pm and $H^{\pm\pm}$ at 1-loop level. Along with that, the doubly charged scalar can participate in processes like $\ell_\alpha \rightarrow \ell_\beta \ell_\gamma \ell_\delta$ even at tree level. The upper limit on the branching fraction of these measurements enables us to determine the allowed region in the $v_t - M_\Delta$ parameter plane. We would like to point out that the mass splitting (ΔM) between the triplet scalars does not directly affect the LFV processes and can be neglected. Following Refs. [31, 38–40], one can realise that the most stringent bound on the aforementioned parameter plane can be obtained while considering the $\mu \rightarrow e \gamma$ [41] and $\mu \rightarrow 3e$ [42] processes. Satisfying the normal (inverted) mass hierarchy conditions, one can determine the following lower limit on v_t depending upon the $m_{H^{\pm\pm}}$ mass -

$$v_t \gtrsim 0.78 - 1.5 (0.69 - 2.9) \times 10^{-8} \text{ GeV} \times \frac{100 \text{ GeV}}{m_{H^{\pm\pm}}}. \quad (15)$$

We now present the updated collider limits for these triplet scalars, which correspond to three different mass hierarchy scenarios. As mentioned before, the triplet scalar masses can be parametrised by using two mass parameters M_Δ and ΔM . We begin with negative and degenerate mass scenarios where the doubly charged scalars can decay either via pure leptonic mode ($H^{\pm\pm} \rightarrow \ell_\alpha^\pm \ell_\beta^\pm$) or via pure vector boson mode ($H^{\pm\pm} \rightarrow W^\pm W^\pm$)⁴.

³One can notice that the parameter λ_4 can be absorbed by redefining \widetilde{M}_Δ while satisfying the identity $M_\Delta^2 = \widetilde{M}_\Delta^2 + \frac{\lambda_4}{2} v_d^2$.

⁴For relatively lighter values of $m_{H^{\pm\pm}}$ one or both of these W bosons can be off-shell.

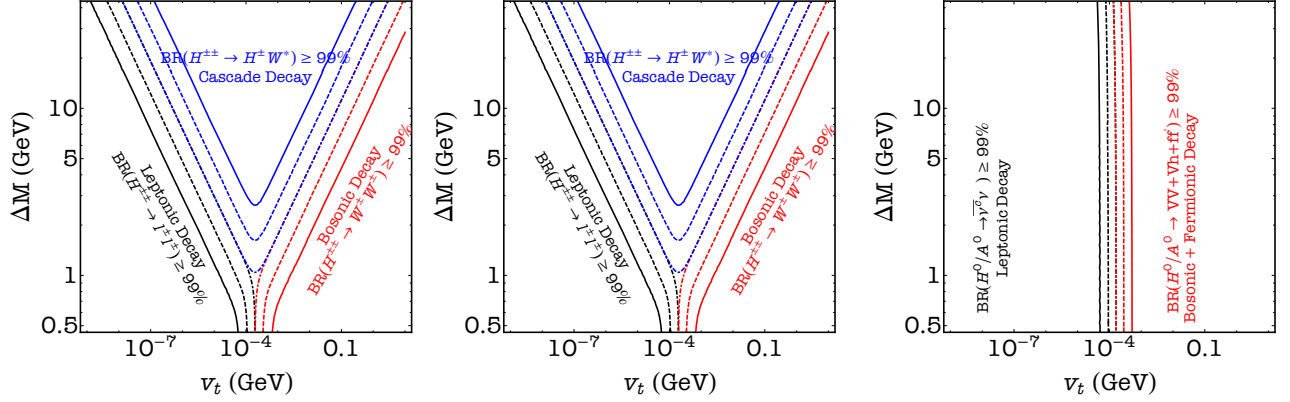


Figure 1: Decay phase diagram of $H^{\pm\pm}$ (left), H^{\pm} (middle), and H^0/A^0 (right) with $m_{H^{\pm\pm}} = 200$ GeV for the positive mass hierarchy scenario. The solid, dashed and dot-dashed contours represent 99%, 95%, and 50% branching ratios in different decay regions.

The vertices between the doubly charged scalar and the charged leptons are roughly proportional to $\sim \frac{m_\nu}{v_t}$. As a result, for $v_t \lesssim \mathcal{O}(10^{-4})$ GeV, these doubly charged scalars dominantly decay via leptonic mode with almost 100% branching ratio. At the LHC, the $H^{\pm\pm}$ bosons can be pair-produced via the Drell–Yan process, leading to pairs of same-sign dilepton final states. This distinctive signature has motivated the experimental collaborations to perform several searches in this channel [11–13, 15–21]. Non-observation of a significant excess *w.r.t.* the SM expectations imposed a stringent bound on the $m_{H^{\pm\pm}}$. The ATLAS collaboration [21] has imposed a lower limit of $m_{H^{\pm\pm}} \lesssim 1020$ GeV for the $H^{\pm\pm} \rightarrow \ell_\alpha^\pm \ell_\alpha^\pm$ final state where $\ell = e, \mu$. Similarly, the CMS collaboration [16] has determined the lower limit $m_{H^{\pm\pm}} \lesssim 535$ GeV for the $H^{\pm\pm} \rightarrow \tau^\pm \tau^\pm$ decay mode.

On the other hand, for $v_t \gtrsim \mathcal{O}(10^{-4})$ GeV, the $H^{\pm\pm} \rightarrow W^\pm W^\pm$ decay mode opens up and in the range of $\mathcal{O}(10^{-3})$ GeV $\lesssim v_t \lesssim \mathcal{O}(1)$ GeV the corresponding branching ratio is almost 100% for $\Delta M \leq 0$. In this scenario, the $H^{\pm\pm}$ scalars can decay into a pair of same-sign W bosons, leading to characteristic collider signatures. Searches by the experimental collaborations [19, 20] have analysed these channels and excluded the mass range 200 GeV $\lesssim m_{H^{\pm\pm}} \lesssim 350$ GeV, depending on the W boson decay mode.

However, the interpretation of the direct search limits significantly alters in the positive mass hierarchy scenario $\Delta M > 0$, where the cascade decay channels open up for both the doubly and singly charged scalars. To elaborate on this, we like to discuss the decays of triplet scalars in more detail. For $\Delta M > 0$, the doubly charged scalars can decay via three possible modes: (i) leptonic decay, $H^{\pm\pm} \rightarrow \ell_i^\pm \ell_j^\pm$, (ii) bosonic modes, $H^{\pm\pm} \rightarrow W^\pm W^\pm$ and (iii) cascade mode, $H^{\pm\pm} \rightarrow H^\pm W^*$ and the ratio between their corresponding branching fractions can be represented approximately in the following manner:

$$\ell\ell : WW : H^\pm W^* :: \left(\frac{m_\nu}{v_t}\right)^2 \left(\frac{v_d}{m_{H^{\pm\pm}}}\right)^2 : \left(\frac{v_t}{v_d}\right)^2 : \frac{\max(\Delta M, 0)^5}{v_d^2 m_{H^{\pm\pm}}^3} \quad (16)$$

We would like to remind that, the mass gap between the triplet scalars has an upper limit of $\Delta M \lesssim 40$ GeV after satisfying the electroweak precision measurements. As a result, the on-shell production of the W is kinematically forbidden. In Fig. 1 *left* panel, we present the branching ratio contours for the $H^{\pm\pm}$ in the v_t - ΔM plane, for the leptonic (black contours), bosonic (red contours), and cascade modes (blue contours), respectively. The solid line encloses the region where the corresponding

BR is roughly around $\geq 99\%$. As expected for lower values of v_t , the doubly charged scalars can decay via leptonic mode, whereas for the large v_t value, the bosonic decay modes dominate. Interestingly, for $\Delta M > 1$ GeV, the cascade decay mode opens up, and it becomes dominant in the region $\Delta M \gtrsim 10$ GeV and 10^{-5} GeV $\lesssim v_t \lesssim 10^{-2}$ GeV.

In the case of singly charged scalars, four possible decay modes open up in the positive mass hierarchy scenario *i.e.* (i) leptonic decay, $H^\pm \rightarrow \tau^\pm \nu$ (ii) hadronic decay, $H^\pm \rightarrow t\bar{b}$, (iii) diboson decay, $H^\pm \rightarrow W^\pm Z/h^0$ and (iv) cascade decay, $H^\pm \rightarrow H^0/A^0 W^*$ respectively. The ratio between the corresponding branching ratios for these channels can be expressed in the following manner:

$$\ell\nu : t\bar{b} : WZ : Wh^0 : H^0/A^0 W^* :: \left(\frac{m_\nu}{v_t}\right)^2 \left(\frac{v_d}{m_{H^\pm}}\right)^2 : \left(\frac{m_t}{v_d}\right)^2 \left(\frac{v_t}{m_{H^\pm}}\right)^2 : \left(\frac{v_t}{v_d}\right)^2 : (1 - 2\zeta)^2 \left(\frac{v_t}{v_d}\right)^2 : \frac{\max(\Delta M, 0)^5}{v_d^2 m_{H^\pm}^3}. \quad (17)$$

Here m_t is the top quark mass and $\zeta = \frac{v_d}{2v_t} \sin \alpha$. In Fig. 1 *central* panel, we illustrate the corresponding branching ratio contours for these channels. For the present discussion, we resort to a minimal mixing between the CP-even scalar states by setting the corresponding value of $\sin \alpha \approx \mathcal{O}(10^{-8})$. From Eq. (17), one can realise that for a nearly mass-degenerate scenario in the region $v_t \lesssim 10^{-4}$ GeV, leptonic decay modes dominate (region enclosed by the solid black contour). Similarly, for the relatively large value of v_t ($v_t \gtrsim 10^{-2}$ GeV), the combination of bosonic and hadronic decay modes surpasses other channels. However, for a moderate range of v_t (10^{-5} GeV $\lesssim v_t \lesssim 10^{-3}$ GeV), the cascade decay modes become the primary channel for the mass gap larger than $\Delta M \gtrsim 10$ GeV.

Apart from the charged scalars, both the CP-even and CP-odd scalars can decay into $\bar{\nu}^c \nu$ a final state, which is described in the *right* panel of Fig. 1. On the other hand, for the large v_t value, these neutral scalars can either decay via bosonic or hadronic modes, depending upon their CP properties as well as the coupling strength that governs those decay modes.

Considering the decay of these triplet scalars, one can realise that for $\Delta M > 0$, there exists a region in the parameter plane that remains excluded from the existing direct search limits as the signal strength corresponding to both the leptonic and hadronic channels is suppressed. In fact, after conducting an elaborate analysis, Refs. [29, 43] have estimated that, in case of the Type-II seesaw model for $\Delta M \gtrsim 10$ GeV and triplet vev ranging between $v_t \approx \mathcal{O}(10^{-7})$ GeV – $\mathcal{O}(10^{-3})$ GeV, remain available after considering all possible theoretical and experimental constraints.

These particular findings serve as the central motivation for our study, where we propose a novel search strategy in the context of the LHC. In Table 1, we mention the corresponding values of relevant parameters that we would like to probe at LHC. As described, in this region of the parameter space, the charged triplet scalars primarily decay via cascade mode and generate off-shell gauge bosons and H^0/A^0 . Due to the off-shell nature, the gauge bosons would further decay into leptons and jets with very low transverse momentum. Furthermore, in this unconstrained region, neutral triplet scalars would exclusively decay to $\bar{\nu}^c \nu$. As an outcome, the final state is populated with soft leptons, soft jets, and very low missing transverse momentum. This particular signature is difficult to probe as it fails to satisfy the triggering criteria of the existing detector. Our primary goal here is to formulate a novel search strategy that can possibly probe this challenging benchmark scenario. In the following section, we will demonstrate the details of our analysis strategy.

Before concluding this section, we would like to remind that for our analysis, M_Δ , ΔM , and v_t are only parameters that are sufficient to describe the corresponding scalar phenomenology. For completeness, we set best-fit values for neutrino oscillation parameters that correspond to the normal

hierarchy. As a result, the corresponding terms of the Y_ν matrix will be fixed accordingly. However, it is important to note that for our present analysis, these oscillation parameters do not play any noticeable role.

M_Δ [GeV]	ΔM [GeV]	v_t [GeV]
[170 GeV, 250 GeV]	[10 GeV, 30 GeV]	10^{-4} GeV

Table 1: *The range of scalar sector parameters that we consider to probe at the LHC.*

4 A cut-and-counts analysis at the LHC

In the context of the Type-II seesaw model, our primary objective in this study is to maximise the sensitivity in the M_Δ - ΔM parameter plane, particularly in regions not yet constrained by existing searches. For that purpose we therefore present a feasibility study for probing the scalar triplet states at the 14 TeV LHC. As described before, we concentrate on a phenomenologically motivated region of parameter space where the doubly charged ($H^{\pm\pm}$) and singly charged scalars (H^\pm) decay predominantly via cascade modes - $H^{\pm\pm} \rightarrow H^\pm W^*$ and $H^\pm \rightarrow HW^*/AW^*$ respectively as described in Fig. 1. The exotic neutral scalars which are produced in these cascades subsequently decay through the invisible channel $H/A \rightarrow \bar{\nu}^c \nu$ mode. To ensure these decay patterns, we set the triplet scalar vev , $v_t \simeq 10^{-4}$ GeV, and the mass gap between the triplet scalars is ranging between 10-30 GeV. At the LHC, the triplet scalars can be inclusively produced via $p p \rightarrow H^{\pm\pm} H^\mp \oplus H^{\pm\pm} H^{\mp\mp} \oplus H^\pm H^\mp$ modes. In the case of a compressed spectra scenario the jets or the leptons which are produced from the off-shell W decay are kinematically soft. Moreover, the neutral scalars produced in the H^\pm decay predominantly yield invisible final states; the characteristic signal topology consists of missing transverse energy (E_T^{miss}) accompanied by soft leptons or jets. For a large fraction of signal events these triplet scalars are pair-produced with negligible transverse boost. As a result, the missing transverse momentum, which is expected from these signal topology becomes negligible, which in turn makes this signal extraction from the corresponding SM background challenging. To overcome this difficulty, we choose following signal process to develop our search strategy -

$$p p \rightarrow H^{\pm\pm} H^\mp j \oplus H^{\pm\pm} H^{\mp\mp} j \oplus H^\pm H^\mp j \quad (18)$$

where the additional hard jet originates from initial state radiation (ISR) [44, 45]. The presence of this hard ISR jet imparts a substantial transverse recoil to the pair of charged triplet scalar system, thereby boosting decay products in the transverse plane. As a result, the otherwise soft and invisible decay products can collectively generate a sizeable missing transverse momentum, E_T^{miss} , which makes the signal experimentally accessible. As discussed, both the singly and doubly charged scalars will decay via cascade mode with a 100% branching ratio and generate additional off-shell W -bosons. For our analysis, we only consider the leptonic decay modes for these off-shell W boson. The primary reason to avoid the hadronic decay modes for these W s is that the jets arise from them fail to pass the reconstruction criteria for the high-luminosity LHC ⁵. The dominant SM backgrounds that are relevant for our present analysis are

- $p p \rightarrow t\bar{t} + \text{jets}$
- $p p \rightarrow W^+ \ell^- \bar{\nu} + \text{jets} + \text{h.c.}$

⁵The minimum transverse momentum threshold required for reliable jet reconstruction is $p_T(j) > 40$ GeV.

- $p p \rightarrow \tau^+ \tau^- + \text{jets}$
- $p p \rightarrow W^+ \ell^+ \ell^- + \text{jets} + \text{h.c.}$
- $p p \rightarrow Z \ell^+ \ell^- + \text{jets}$
- $p p \rightarrow tW$,

In all these cases, the final-state neutrinos can give rise to the E_T^{miss} spectrum, and *+jets* denote both the one-jet and two-jet events. To generate the signal process, we incorporate the Type-II seesaw Lagrangian in FEYNRULESv2.3.x [46] and develop the required UFO files. We use the Madgraph5@NLOv2.9.21 [47] to simulate both the signal and background events with the NNPDF23 L0 [48] parton distribution function. At the parton-level event generation, we demand at least one jet with $p_T^j > 100$ GeV. This choice effectively suppresses low-energy QCD backgrounds while simultaneously providing a substantial transverse recoil to the charged triplet scalar system. All the cross sections are calculated at tree level. After the parton-level generation, the simulated events are passed to PYTHIA8 [49] to incorporate the showering and hadronization effects. The detector level simulation is performed using DELPHESv3.5.0 [50] with the help of appropriate card that enable us to use low p_T leptons. To evade the double counting, we use the MLM scheme for the jet matching and merging [51]. To reconstruct various objects that are present in the final state we use the following criteria.

Jets are reconstructed using the **Fastjet** package [52] with the anti- k_T algorithm and jet radius parameter $R = 0.4$. All jets are required to be hadronic clusters satisfying $|\eta| < 5$ and $p_T > 40$ GeV.

In the present analysis, the final signal state consists of kinematically soft leptons ($\ell = e, \mu$) satisfying $|\eta| < 2.5$ and $p_\ell \geq 5$ GeV. The tagging efficiencies are taken from the detector card `CMS_PhaseII_OPU.tcl` provided with DELPHESv3.5.0.

Hadronic clusters are identified as b -jets if they contain a B -hadron with $p_T(b) > 20$ GeV and $|\eta| \leq 3.4$. The b -tagging and misidentification efficiencies are taken from the card `btagMedium.tcl`.

Similarly, hadronic tau leptons (τ_h) are identified with the kinematic requirements $p_T(\tau_h) > 20$ GeV and $|\eta(\tau_h)| < 2.3$. The tau-tagging efficiencies are implemented using the parameterized functions of p_T and η provided in the card `CMS_PhaseII_OPU.tcl`.

Finally, to calculate the statistical significance for our analysis, we use the following formula

$$\mathcal{Z} = \frac{\sqrt{\mathcal{L}}\sigma_S}{\sqrt{\sigma_S + \sigma_B}}. \quad (19)$$

We begin our analysis by employing a b -quark veto cut where we assume medium tagging efficiency consistent with current LHC detector performance. This veto plays an important role in rejecting those backgrounds which have top quark in the final state. With this cut, we can reject approximately one-third of top-associated background events while nominally affecting the signal events, which typically fail to contain heavy flavor quarks. In a similar spirit, we impose a veto on hadronically decaying τ_h . Using this veto we can suppress around 40% of the tau-pair background events while marginally affecting signal and other background processes. Furthermore we select those events that consist with single jet in the final state topology. These particular selection cuts significantly reduce

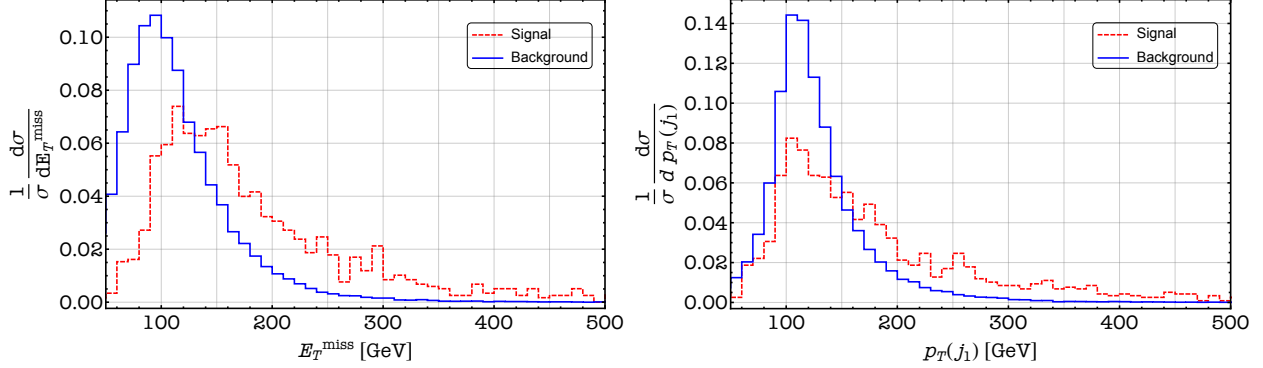


Figure 2: Normalized differential distribution corresponds to missing transverse momentum E_T^{miss} (left) and the leading transverse momentum of the jet $p_T(j_1)$ for the signal and the total SM background. The solid blue line and the red dashed line represents the signal and the total SM background respectively.

the $t\bar{t}$ +jets and $W\ell\nu$ +jets background as highlighted in Table 3. With these selection criteria in hand, we now consider different kinematic distributions to further improve our signal background efficiency.

In Fig. 2, we demonstrate the normalized distribution correspond to E_T^{miss} (left) and leading jet $p_T(j_1)$ (right) respectively. At the generation level, we have imposed an inclusive criterion with $p_T^j > 100$ GeV. As a result one can notice that the majority of signal and background events are distributed in the high p_T value. In contrast, if we consider the E_T^{miss} distribution, for the signal events the emitted hard jet would give rise to the large missing transverse energy for the triplet-pair system. As a result one can find a similarity between the shape of E_T^{miss} and $p_T(j_1)$ for the signal. On the other hand, this correlation between both these distributions does not appear for the SM backgrounds, which motivate us to devise the following cuts to distinguish the signal from backgrounds

$$E_T^{miss} > 120 \text{ GeV} \ \& \ p_T(j_1) > 120 \text{ GeV} \ \text{with} \ |\eta(j_1)| \leq 2.5. \quad (20)$$

After applying the aforementioned kinematic cuts, we further demand the presence of two leptons in the final state. We like to point out that the lepton tagging efficiency primarily depends on their corresponding transverse momentum, and if it's $p_T^\ell < 5$ GeV, then corresponding tagging efficiency is zero. In addition to the range $5 \text{ GeV} < p_T^\ell < 10 \text{ GeV}$, the tagging efficiency roughly varies between 50% to 70% depending on detector performance. As a result by demanding these di-lepton ($N_\ell = 2$) systems in practice, only 10% of the signal events survive. Nevertheless, this requirement is essential to suppress purely hadronic backgrounds and to maintain a clean experimental signature.

At this stage of analysis, the $\tau^+\tau^-$ +jets process emerges as the dominant SM background, which makes the signal extraction from the background challenging. Hence, we adopt the di-tau invariant mass observable, which was described in Ref. [45]. Before defining this variable, we'd like to elaborate on the $\tau^+\tau^-$ +jets background. For these SM process both these τ pairs are produced due to the decay of highly boosted Z -bosons. On top of that, we assume that both these tau lepton is further decay via pure leptonic mode $\tau \rightarrow \ell\nu\bar{\nu}$. Since the parent τ 's are produced with an ultra-relativistic momentum, all the daughter particles that arise from the τ decays would be expected to be collimated towards the parent particle's direction. Additionally one can expect that the neutrinos produced from the individual τ decay carry the momentum of $\xi_1 p_T(\ell_1)$ and $\xi_2 p_T(\ell_2)$ respectively. Here, both the ξ_i represent the momentum fraction carries by the neutrinos towards the transverse plane and ℓ_i are the

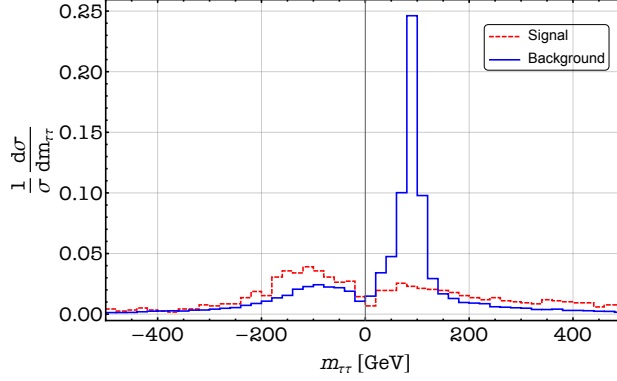


Figure 3: Normalized differential distribution corresponds to $m_{\tau\tau}$ variables for the signal and the total SM background. The solid blue line and the red dashed line represents the signal and the total SM background respectively.

leptons produced from each of the parent τ . Considering the momentum conservation in the transverse plane for the Zj system, we can write down the following identity:

$$-p_T(j_1) = (1 + \xi_1)p_T(\ell_1) + (1 + \xi_2)p_T(\ell_2) \quad (21)$$

In principle, Eq. (21) comprises independent equations, and using the measured value of $p_T(j_1)$, it is possible to calculate the actual value ξ_i for the event-by-event level. With the collinear tau decay approximation, the corresponding invariant mass for the di-tau system can be expressed as

$$m_{\tau\tau}^2 = m_{\ell_1\ell_2}^2(1 + \xi_1)(1 + \xi_2) \quad (22)$$

where $m_{\ell_1\ell_2}^2$ signifies the invariant squared mass of leading and sub-leading leptons. In Fig. 3, we illustrate the normalized distribution of $m_{\tau\tau}$ variable which is defined as $m_{\tau\tau} \equiv \text{Sign}[m_{\tau\tau}^2] \times \sqrt{|m_{\tau\tau}^2|}$. For the background events, one can notice a sharp peak at the Z -boson pole mass value, which arises from the di-tau system. In contrast, for the signal and other SM backgrounds, the E_T^{miss} direction and leptons' momentum direction are uncorrelated, and the events are distributed over the entire range of $m_{\tau\tau}$. Our primary objective here is to reject all those events which are from Z boson decay. Along with that, to achieve further sensitivity, we only select those events that satisfy the following criteria:

$$m_{\tau\tau} > 200 \text{ GeV and } m_{\tau\tau} < -100 \text{ GeV} \quad (23)$$

With this cut, one can reject the majority of the $\tau\tau$ +jets events, which dominantly reside around the Z -boson mass pole. In addition, the $t\bar{t}$ +jets events are also lying around $-100 \text{ GeV} < m_{\tau\tau} < 200 \text{ GeV}$ bins. These guide us to devise a asymmetrical cut for this variable.

After implementing all these cuts, the total number of surviving signal events is substantially reduced. At this point, our objective is to find suitable kinematic variables that can suppress the residual background without significantly affecting the signal events. To achieve this goal, we like to examine the kinematics of the leptons that are present in the final state. In the case of the signal, the leptons are produced due to subsequent decays of off-shell W -bosons. For moderately small values of ΔM , leptons are expected to be relatively soft. In Fig. 4, we present the normalized distribution corresponding to the leading lepton $p_T(\ell_1)$ (left) and vector sum of leptons, $\sum p_T(\ell)$, respectively. As expected, for both these variables, the majority of the signal events populate the low p_T region. In

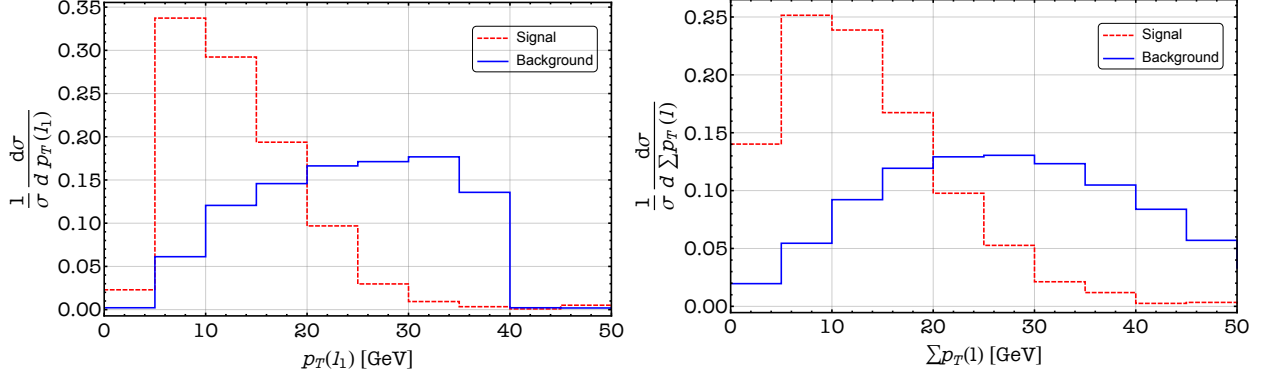


Figure 4: Normalized differential distribution corresponds to the leading transverse momentum of the jet $p_T(\ell_1)$ (left) and the vector sum of lepton transverse momentum $\sum_{i=1,2} p_T(\ell_i)$ for the signal and the total SM background. The solid blue line represents the total SM background, and the red dashed line represents the signal, respectively.

contrast, for the dominant backgrounds, the leptons are typically produced from on-shell gauge bosons and therefore exhibit harder transverse momentum spectra. Motivated by the distributions shown in Fig. 4, we therefore impose the following upper bounds on the transverse momentum of the leading lepton, $p_T(\ell)$, as well as on the scalar sum of lepton transverse momenta, $\sum p_T(\ell)$

$$p_T(\ell_1) < 20 \text{ GeV} \quad \text{and} \quad \sum_{i=1,2} p_T(\ell_i) < 25 \text{ GeV}. \quad (24)$$

These requirements significantly suppress the residual backgrounds while retaining a sizable fraction of the signal events, particularly in the compressed mass spectrum regime under consideration. We emphasize that these cuts are specifically designed to target the soft-lepton signature intrinsic to the cascade decay topology of the Type-II seesaw scalars and are complementary to the previously imposed E_T^{miss} , ISR jet, and $m_{\tau\tau}$ selection.

Cut-0	Initial cross section
Cut-1	b -quark veto
Cut-2	τ_h veto
Cut-3	$N_j = 1$
Cut-4	$p_T(j_1) > 120 \text{ GeV}$ and $ \eta(j_1) $
Cut-5	$E_T^{miss} > 120 \text{ GeV}$
Cut-6	$N_\ell = 2$
Cut-7	$m_{\tau\tau} > 200 \text{ GeV}$ and $m_{\tau\tau} < -100 \text{ GeV}$
Cut-8	$p_T(\ell_1) < 20 \text{ GeV}$
Cut-9	$\sum_{i=1,2} p_T(\ell_i) < 25 \text{ GeV}$

Table 2: Definition of cuts that are implemented in the signal background analysis.

The cumulative effect of all selection cuts is summarized in Table 3 for $\Delta M = 10 \text{ GeV}$ and 30 GeV , respectively, where we present the cut-flow for both the signal and the relevant SM backgrounds.

As evident from this table, the combination of all the cuts leads to a substantial suppression of the background while maintaining a non-negligible signal yield. In particular, the $\tau^+\tau^-$ +jets and $t\bar{t}$ +jets backgrounds are efficiently reduced at successive stages of the analysis, resulting in a significantly improved signal-to-background ratio in the final selection.

	(200, 10) [GeV] [fb]	(200, 30) [GeV] [fb]	$t\bar{t}$ + jets [fb]	$\tau\tau$ + jets [fb]	WW + jets [fb]	$Z\ell\ell$ + jets [fb]	$W\ell\ell$ + jets [fb]	tW [fb]
Cut-0	25.55	20	4.0214×10^4	2.2237×10^4	3.267×10^3	107.07	390.219	1.42×10^4
Cut-1	23.61	17.746	9.57×10^3	2.0772×10^4	2.945×10^3	87.56	347.49	5.95×10^3
Cut-2	23.038	16.576	8.847×10^3	1.2576×10^4	2.782×10^3	82.486	324.814	5.67×10^3
Cut-3	9.543	3.79	99.433	2.111×10^3	113.92	0.9054	2.299	1.08×10^3
Cut-4	5.668	2.13	45.4503	646.958	50.248	0.405	0.9402	50.065
Cut-5	5.282	1.862	32.8601	284.715	39.078	0.3417	0.5916	30.97
Cut-6	0.363	0.364	12.3326	47.044	12.952	0.2394	0.2766	10.8775
Cut-7	0.2606	0.272	9.9981	4.567	10.168	0.141	0.1878	4.9875
Cut-8	0.2135	0.1396	2.7209	2.0416	2.2617	0.0561	0.0792	0.9975
Cut-9	0.2044	0.1304	2.3023	1.8304	1.827	0.048	0.0714	0.855

Table 3: Summary of effective cross-section for the signal and dominant background at a 14 TeV pp collider. For the signal process, we set the singly charged scalar mass at $M_\Delta = 200$ GeV and the triplet scalar mass gap $\Delta M = 10$ GeV and 30 GeV. The second row highlights the initial cross section after demanding at least one jet with $p_T^j \geq 100$ GeV and MLM matching.

Using the final event yields after all cuts, we evaluate the statistical significance for different combinations of ΔM and M_Δ values following the prescription described in Eq. (19). Based on this analysis, we derive the projected sensitivity at the 14 TeV LHC in the $M_\Delta - \Delta M$ parameter plane as shown in Fig. 5 for integrated luminosity $\mathcal{L} = 3000$ fb^{-1} . The blue shaded region represents 5σ discovery, and the red shaded region represents 2σ exclusion reach for the proposed analysis. As evident from this figure, our strategy exhibits significant sensitivity in the moderately compressed regime, particularly for mass splitting in the range 10 GeV $\lesssim \Delta M \lesssim 30$ GeV. The reach extends up to $M_\Delta \sim 220$ -230 GeV at the 2σ level, while a robust 5σ discovery is achievable for comparatively lower triplet masses roughly around $M_\Delta \lesssim 190$ GeV, depending on the exact value of ΔM . We like to remind you that for this analysis we set the triplet vev at $v_t = 10^{-4}$ GeV. The sensitivity degrades for very small mass splitting, where the decay products become extremely soft and fail to satisfy the lepton reconstruction thresholds, as well as for larger ΔM , where the leptons become harder, and the signal begins to resemble SM backgrounds more closely. In addition, for a large value of M_Δ , the initial signal cross section, it is significantly low to achieve desirable sensitivity. This demonstrates that ISR-assisted searches provide a powerful and complementary avenue to explore compressed triplet scalar spectra in the Type-II seesaw model. The results highlight the importance of dedicated analyses targeting such challenging regions of parameter space, which may otherwise remain elusive in standard high- p_T searches.

5 Summary and Conclusions

In this work, we have revisited the collider phenomenology of the Type-II seesaw model with a particular focus on regions of parameter space that remain weakly constrained by existing experimental searches. Current limits on the mass of the doubly charged Higgs boson are largely derived under the assumption

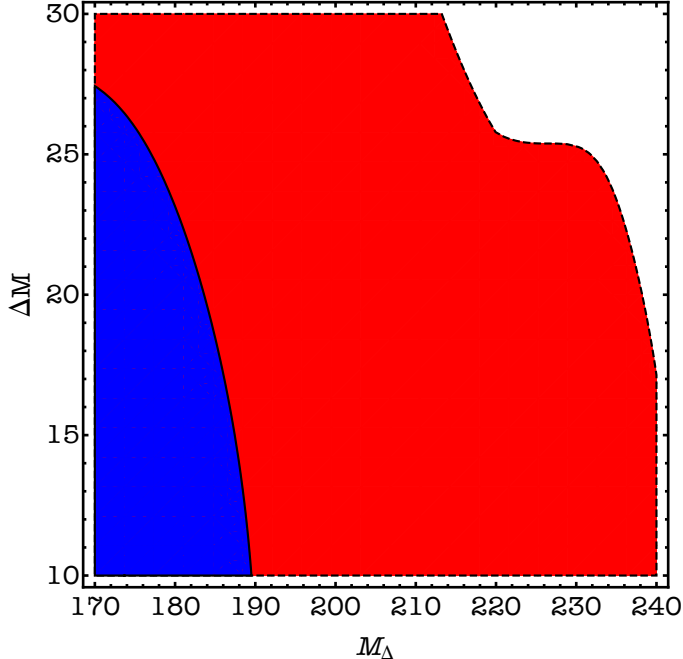


Figure 5: *Projected sensitivity in the $M_\Delta - \Delta M$ plane after applying the cut-based analysis of the signal and background distribution at the 14 TeV LHC. The black dashed and solid black curves correspond to 2σ exclusion and 5σ discovery contours, respectively, assuming an integrated luminosity of $\mathcal{L} = 3000 \text{ fb}^{-1}$. The shaded region indicates the parameter space where signal significance exceeds the corresponding confidence level, with the red (blue) shaded region representing 2σ (5σ) sensitivity reaches. The unshaded region can not be probed using the present analysis assumptions.*

that its decays are dominated either by same-sign dilepton or same-sign diboson final states. However, as emphasized in recent studies and demonstrated in this analysis, such assumptions are not generic once moderate mass splittings among the triplet scalars are taken into account. In the presence of compressed spectra, cascade decays such as these $H^{\pm\pm} \rightarrow H^\pm W^\pm$ become dominant, while the conventional leptonic and bosonic decay modes are suppressed.

We have shown that this suppression arises from two intertwined effects: the reduced phase space available for direct decays of the doubly charged scalar and the softness of the visible decay products emerging from the cascade chains. In particular, for moderate mass splitting of $10 \text{ GeV} \lesssim \Delta M \lesssim 30 \text{ GeV}$ and triplet vev ranging between $10^{-5} \text{ GeV} \lesssim v_t \lesssim 10^{-3} \text{ GeV}$, the decay widths of $H^{\pm\pm} \rightarrow \ell^\pm \ell^\pm$ and $H^{\pm\pm} \rightarrow W^\pm W^\pm$ become subdominant. At the same time, the subsequent decays of the charged and neutral triplet scalars predominantly yield soft leptons and missing transverse energy, rendering standard search strategies largely ineffective. Consequently, sizeable regions of the Type-II seesaw parameter space remain unconstrained despite stringent bounds reported by the ATLAS and CMS collaborations.

Motivated by these challenges, we proposed a dedicated collider search strategy specifically tailored to this elusive regime. Our analysis exploits the presence of a hard initial-state radiation jet to boost the triplet scalar system, thereby generating a detectable missing transverse momentum signature. The signal is characterized by missing energy accompanied by soft leptons originating from off-shell W bosons produced in the cascade decays of the charged scalars, as well as neutrino-dominated decays of the neutral states. By combining object-level vetoes, kinematic selections, an asymmetric

di-tau invariant mass cut to suppress the $\tau^+\tau^- + \text{jets}$ background, and requirements exploiting the softness of the leptons, we demonstrated that the signal can be efficiently separated from the dominant SM backgrounds within a cut-and-count framework.

Our results show that, at the 14 TeV LHC, meaningful evidence-level and discovery-level sensitivities can be achieved in regions of the $M_\Delta - \Delta M$ parameter plane that are currently poorly constrained. In particular, we can achieve a 5σ discovery sensitivity for triplet scalar masses in the range 170 GeV - 190 GeV, with mass gap varying between 10 GeV and 25 GeV. This proposed strategy significantly extends the experimental reach into the moderately compressed regime, highlighting its complementarity to existing searches optimized for hard leptonic or bosonic final states. Overall, this study underscores the importance of accounting for cascade-dominated decay topologies and compressed spectra when interpreting collider limits on extended scalar sectors. Dedicated searches of the kind presented here will be essential for fully probing the Type-II seesaw model and, more broadly, for uncovering collider signatures associated with the origin of neutrino masses at present and future runs of the LHC.

Acknowledgments

TG would like to thank Alexandre Alves, Kuver Sinha and Antonio Oliveira for useful discussions during the early stages of this project. AS thanks Anusandhan National Research Foundation (ANRF) for providing the necessary financial support through the SERB-NPDF grant (Ref. No.: PDF/2023/002572). AS and TG acknowledges the support from the Department of Atomic Energy (DAE), India, for the Regional Centre for Accelerator-based Particle Physics (RECAPP), Harish Chandra Research Institute. AD thanks the Carl Trygger Foundation for the support under the project CTS 23:2930.

References

- [1] W. Konetschny and W. Kummer, *Nonconservation of Total Lepton Number with Scalar Bosons*, *Phys. Lett. B* **70** (1977) 433.
- [2] T.P. Cheng and L.-F. Li, *Neutrino Masses, Mixings and Oscillations in $SU(2) \times U(1)$ Models of Electroweak Interactions*, *Phys. Rev. D* **22** (1980) 2860.
- [3] G. Lazarides, Q. Shafi and C. Wetterich, *Proton Lifetime and Fermion Masses in an $SO(10)$ Model*, *Nucl. Phys. B* **181** (1981) 287.
- [4] J. Schechter and J.W.F. Valle, *Neutrino Masses in $SU(2) \times U(1)$ Theories*, *Phys. Rev. D* **22** (1980) 2227.
- [5] R.N. Mohapatra and G. Senjanovic, *Neutrino Masses and Mixings in Gauge Models with Spontaneous Parity Violation*, *Phys. Rev. D* **23** (1981) 165.
- [6] M. Magg and C. Wetterich, *Neutrino Mass Problem and Gauge Hierarchy*, *Phys. Lett. B* **94** (1980) 61.
- [7] ATLAS collaboration, *Observation of a new particle in the search for the Standard Model Higgs boson with the ATLAS detector at the LHC*, *Phys. Lett. B* **716** (2012) 1 [[1207.7214](#)].
- [8] CMS collaboration, *Observation of a New Boson at a Mass of 125 GeV with the CMS Experiment at the LHC*, *Phys. Lett. B* **716** (2012) 30 [[1207.7235](#)].

- [9] ATLAS collaboration, *A detailed map of Higgs boson interactions by the ATLAS experiment ten years after the discovery*, *Nature* **607** (2022) 52 [2207.00092].
- [10] CMS collaboration, *A portrait of the Higgs boson by the CMS experiment ten years after the discovery.*, *Nature* **607** (2022) 60 [2207.00043].
- [11] ATLAS collaboration, *Search for doubly-charged Higgs bosons in like-sign dilepton final states at $\sqrt{s} = 7$ TeV with the ATLAS detector*, *Eur. Phys. J. C* **72** (2012) 2244 [1210.5070].
- [12] CMS collaboration, *A Search for a Doubly-Charged Higgs Boson in pp Collisions at $\sqrt{s} = 7$ TeV*, *Eur. Phys. J. C* **72** (2012) 2189 [1207.2666].
- [13] ATLAS collaboration, *Search for anomalous production of prompt same-sign lepton pairs and pair-produced doubly charged Higgs bosons with $\sqrt{s} = 8$ TeV pp collisions using the ATLAS detector*, *JHEP* **03** (2015) 041 [1412.0237].
- [14] CMS collaboration, *Study of vector boson scattering and search for new physics in events with two same-sign leptons and two jets*, *Phys. Rev. Lett.* **114** (2015) 051801 [1410.6315].
- [15] CMS collaboration, *Search for a doubly-charged Higgs boson with $\sqrt{s} = 8$ TeV pp collisions at the CMS experiment*, .
- [16] CMS collaboration, *A search for doubly-charged Higgs boson production in three and four lepton final states at $\sqrt{s} = 13$ TeV*, .
- [17] ATLAS collaboration, *Search for doubly charged Higgs boson production in multi-lepton final states with the ATLAS detector using proton–proton collisions at $\sqrt{s} = 13$ TeV*, *Eur. Phys. J. C* **78** (2018) 199 [1710.09748].
- [18] CMS collaboration, *Observation of electroweak production of same-sign W boson pairs in the two jet and two same-sign lepton final state in proton-proton collisions at $\sqrt{s} = 13$ TeV*, *Phys. Rev. Lett.* **120** (2018) 081801 [1709.05822].
- [19] ATLAS collaboration, *Search for doubly charged scalar bosons decaying into same-sign W boson pairs with the ATLAS detector*, *Eur. Phys. J. C* **79** (2019) 58 [1808.01899].
- [20] ATLAS collaboration, *Search for doubly and singly charged Higgs bosons decaying into vector bosons in multi-lepton final states with the ATLAS detector using proton-proton collisions at $\sqrt{s} = 13$ TeV*, *JHEP* **06** (2021) 146 [2101.11961].
- [21] ATLAS collaboration, *Search for doubly charged Higgs boson production in multi-lepton final states using 139 fb^{-1} of proton–proton collisions at $\sqrt{s} = 13$ TeV with the ATLAS detector*, *Eur. Phys. J. C* **83** (2023) 605 [2211.07505].
- [22] S. Antusch, O. Fischer, A. Hammad and C. Scherb, *Low scale type II seesaw: Present constraints and prospects for displaced vertex searches*, *JHEP* **02** (2019) 157 [1811.03476].
- [23] T.B. de Melo, F.S. Queiroz and Y. Villamizar, *Doubly Charged Scalar at the High-Luminosity and High-Energy LHC*, *Int. J. Mod. Phys. A* **34** (2019) 1950157 [1909.07429].
- [24] R. Primulando, J. Julio and P. Uttayarat, *Scalar phenomenology in type-II seesaw model*, *JHEP* **08** (2019) 024 [1903.02493].

- [25] E.J. Chun, S. Khan, S. Mandal, M. Mitra and S. Shil, *Same-sign tetralepton signature at the Large Hadron Collider and a future pp collider*, *Phys. Rev. D* **101** (2020) 075008 [1911.00971].
- [26] Y. Cai, T. Han, T. Li and R. Ruiz, *Lepton Number Violation: Seesaw Models and Their Collider Tests*, *Front. in Phys.* **6** (2018) 40 [1711.02180].
- [27] F.F. Deppisch, P.S. Bhupal Dev and A. Pilaftsis, *Neutrinos and Collider Physics*, *New J. Phys.* **17** (2015) 075019 [1502.06541].
- [28] S. Ashanujjaman and K. Ghosh, *Revisiting type-II see-saw: present limits and future prospects at LHC*, *JHEP* **03** (2022) 195 [2108.10952].
- [29] S. Ashanujjaman and S.P. Maharathy, *Probing compressed mass spectra in the type-II seesaw model at the LHC*, *Phys. Rev. D* **107** (2023) 115026 [2305.06889].
- [30] P.S. Bhupal Dev, D.K. Ghosh, N. Okada and I. Saha, *125 GeV Higgs Boson and the Type-II Seesaw Model*, *JHEP* **03** (2013) 150 [1301.3453].
- [31] P.S.B. Dev, C.M. Vila and W. Rodejohann, *Naturalness in testable type II seesaw scenarios*, *Nucl. Phys. B* **921** (2017) 436 [1703.00828].
- [32] PARTICLE DATA GROUP collaboration, *Review of Particle Physics*, *PTEP* **2020** (2020) 083C01.
- [33] I. Esteban, M.C. Gonzalez-Garcia, M. Maltoni, T. Schwetz and A. Zhou, *The fate of hints: updated global analysis of three-flavor neutrino oscillations*, *JHEP* **09** (2020) 178 [2007.14792].
- [34] A. Melfo, M. Nemevsek, F. Nesti, G. Senjanovic and Y. Zhang, *Type II Seesaw at LHC: The Roadmap*, *Phys. Rev. D* **85** (2012) 055018 [1108.4416].
- [35] E.J. Chun, H.M. Lee and P. Sharma, *Vacuum Stability, Perturbativity, EWPD and Higgs-to-diphoton rate in Type II Seesaw Models*, *JHEP* **11** (2012) 106 [1209.1303].
- [36] M. Aoki, S. Kanemura, M. Kikuchi and K. Yagyu, *Radiative corrections to the Higgs boson couplings in the triplet model*, *Phys. Rev. D* **87** (2013) 015012 [1211.6029].
- [37] GFITTER GROUP collaboration, *The global electroweak fit at NNLO and prospects for the LHC and ILC*, *Eur. Phys. J. C* **74** (2014) 3046 [1407.3792].
- [38] D.N. Dinh, A. Ibarra, E. Molinaro and S.T. Petcov, *The $\mu - e$ Conversion in Nuclei, $\mu \rightarrow e\gamma$, $\mu \rightarrow 3e$ Decays and TeV Scale See-Saw Scenarios of Neutrino Mass Generation*, *JHEP* **08** (2012) 125 [1205.4671].
- [39] A.G. Akeroyd, M. Aoki and H. Sugiyama, *Lepton Flavour Violating Decays $\tau \rightarrow \text{anti-}l \text{ } l$ and $\mu \rightarrow e \text{ } \gamma$ in the Higgs Triplet Model*, *Phys. Rev. D* **79** (2009) 113010 [0904.3640].
- [40] M. Kakizaki, Y. Ogura and F. Shima, *Lepton flavor violation in the triplet Higgs model*, *Phys. Lett. B* **566** (2003) 210 [hep-ph/0304254].
- [41] MEG collaboration, *Search for the lepton flavour violating decay $\mu^+ \rightarrow e^+ \gamma$ with the full dataset of the MEG experiment*, *Eur. Phys. J. C* **76** (2016) 434 [1605.05081].
- [42] SINDRUM collaboration, *Search for the Decay $\mu^+ \rightarrow e^+ e^+ e^-$* , *Nucl. Phys. B* **299** (1988) 1.

- [43] S. Ashanujjaman, P.S.B. Dev, J. Huang and S. Zhou, *Precision Higgs Probe of Type-II Seesaw*, [2512.07532](#).
- [44] H. Baer, A. Mustafayev and X. Tata, *Monojet plus soft dilepton signal from light higgsino pair production at LHC14*, *Phys. Rev. D* **90** (2014) 115007 [[1409.7058](#)].
- [45] B. Dutta, K. Fantahun, A. Fernando, T. Ghosh, J. Kumar, P. Sandick et al., *Probing Squeezed Bino-Slepton Spectra with the Large Hadron Collider*, *Phys. Rev. D* **96** (2017) 075037 [[1706.05339](#)].
- [46] A. Alloul, N.D. Christensen, C. Degrande, C. Duhr and B. Fuks, *FeynRules 2.0 - A complete toolbox for tree-level phenomenology*, *Comput. Phys. Commun.* **185** (2014) 2250 [[1310.1921](#)].
- [47] J. Alwall, R. Frederix, S. Frixione, V. Hirschi, F. Maltoni, O. Mattelaer et al., *The automated computation of tree-level and next-to-leading order differential cross sections, and their matching to parton shower simulations*, *JHEP* **07** (2014) 079 [[1405.0301](#)].
- [48] R.D. Ball et al., *Parton distributions with LHC data*, *Nucl. Phys. B* **867** (2013) 244 [[1207.1303](#)].
- [49] C. Bierlich et al., *A comprehensive guide to the physics and usage of PYTHIA 8.3*, *SciPost Phys. Codeb.* **2022** (2022) 8 [[2203.11601](#)].
- [50] DELPHES 3 collaboration, *DELPHES 3, A modular framework for fast simulation of a generic collider experiment*, *JHEP* **02** (2014) 057 [[1307.6346](#)].
- [51] M.L. Mangano, M. Moretti, F. Piccinini and M. Treccani, *Matching matrix elements and shower evolution for top-quark production in hadronic collisions*, *JHEP* **01** (2007) 013 [[hep-ph/0611129](#)].
- [52] M. Cacciari, G.P. Salam and G. Soyez, *FastJet User Manual*, *Eur. Phys. J. C* **72** (2012) 1896 [[1111.6097](#)].